Interfacial Design and Mechanical Optimization of Cu18150/Al1060/Cu18150 Trilayer Metallic Composites via Tailored Annealing after High-Temperature Oxygen-Free Rolling

Yuchao Zhao , Mahmoud Ebrahimi , Linfeng Wu , Shokouh Attarilar , Qudong Wang *

Posted Date: 2 January 2026

doi: 10.20944/preprints202601.0095.v1

Keywords: copper-aluminum composite; high-temperature oxygen-free rolling; heat treatment; intermetallic compounds; diffusion kinetics; tensile properties; fracture mechanism

 doi:10.20944/preprints202601.0095.v1

Article

Interfacial Design and Mechanical Optimization of Cu18150/Al1060/Cu18150 Trilayer Metallic Composites via Tailored Annealing After High-Temperature Oxygen-Free Rolling

Yuchao Zhao [1], Mahmoud Ebrahimi [2], Linfeng Wu [1], Shokouh Attarilar [3] and Qudong Wang [1,*]

[1] National Engineering Research Center of Light Alloy Net Forming and Key State Laboratory of Metal Matrix Composites, School of Material Science and Engineering, Shanghai Jiao Tong University, Shanghai, 200240, China

[2] Department of Mechanical Engineering, Faculty of Engineering, University of Maragheh, Maragheh, 83111-55181, Iran

[3] Department of Materials Engineering, Faculty of Engineering, University of Maragheh, Maragheh, 83111-55181, Iran

* Correspondence: wangqudong@sjtu.edu.cn

Abstract

Copper-aluminum layered composites offer a promising combination of high conductivity, light weight, and cost-effectiveness, making them attractive for applications in electric vehicles, electronics, and power transmission. However, achieving reliable interfacial bonding while avoiding excessive work hardening and brittle intermetallic formation remains a significant challenge. In this study, a Cu18150/Al1060/Cu18150 trilayer composite was fabricated through a three-stage high-temperature oxygen-free rolling process. Subsequently, the produced composite was subjected to annealing treatments to systematically investigate the effects of rolling passes, annealing temperature/time on interfacial evolution and mechanical behavior. Results indicate that rolling passes primarily influence interfacial topography and defect distribution. Fewer passes lead to wavy, mechanically bonded interfaces, while more passes improve flatness but reduce intermetallic continuity. Annealing temperature critically governs diffusion kinetics; temperatures up to 400 °C promote the formation of a uniform Al_2Cu layer, whereas 450 °C accelerates the growth of brittle Al_4Cu_9, thickening the intermetallic layer to 18 μm and compromising toughness. Annealing duration further modulates diffusion mechanisms, with short-term (0.5 h) treatments favoring defect-assisted diffusion, resulting in a porous, rapidly thickened layer. In contrast, longer annealing (≥1 h) shifts toward lattice diffusion, which densifies the interface but risks excessive brittle phase formation if prolonged. Mechanical performance evolves accordingly; as-rolled strength increases with the number of rolling passes, but at the expense of ductility. Annealing transforms bonding from a mechanical to a metallurgical condition, shifting fracture from delamination to collaborative failure. The identified optimal process, single-pass rolling followed by annealing at 420°C for 1 hour, yields a balanced interfacial structure of Al_2Cu, AlCu, and Al_4Cu_9 phases, achieving a tensile strength of 258.9 MPa and an elongation of 28.2%, thereby satisfying the target performance criteria (≥220 MPa and ≥20%).

Keywords: copper-aluminum composite; high-temperature oxygen-free rolling; heat treatment; intermetallic compounds; diffusion kinetics; tensile properties; fracture mechanism

 doi:10.20944/preprints202601.0095.v1

1. Introduction

The pursuit of high-performance, multifunctional materials has become a cornerstone of modern materials engineering in response to the global imperative for energy efficiency, lightweight design, and sustainability. Across diverse sectors, including transportation, renewable energy, high-speed electronics, etc., there is mounting pressure to develop materials that combine low density, high strength, and superior electrical/thermal conductivities within a single architecture [1]. This necessity stems from the accelerating shift toward electrification and miniaturization, where the careful management of heat and current under demanding mechanical conditions dictates device longevity and system efficiency. Against this evolving backdrop, heterogeneous metallic composites such as Cu/Al multilayers have emerged as promising solutions, offering an engineered balance between functional and structural properties that cannot be achieved by monolithic metals alone [2–4].

Copper, with an electrical conductivity of approximately 5.96×10^7 S/m and thermal conductivity near 401 W/m·K, remains indispensable for high-performance electrical and thermal applications [5]. Its excellent corrosion resistance and mechanical integrity under varying environments make it the preferred choice in power transmission, heat exchangers, and electronic packaging. However, its high density (8.96 g/cm^3) presents a recurring challenge for applications where weight directly impacts performance, such as in electric vehicles, aerospace structures, and portable electronics. Moreover, the fluctuating price of copper compounds the economic constraints associated with large-scale deployment [6,7]. In contrast, aluminum offers a markedly lower density (2.70 g/cm^3), roughly one-third of that of copper, along with a cost advantage and moderate thermal and electrical conductivities (≈3.5×10^7 S/m and 237 W/m·K, respectively). These attributes have made it attractive for lightweight electrical conductors and structural materials. Nonetheless, aluminum's lower mechanical strength, higher creep rate, and pronounced oxidation tendency often limit its standalone use where high reliability under thermal and mechanical loads is required [8].

The practical and economic advantages of combining these two metals have long been recognized. The concept of copper–aluminum composites aims to harness the high conductivity and strength of copper with the lightweight and cost-effectiveness of aluminum. In a layered architecture, copper surfaces provide excellent electrical contact, wear resistance, and corrosion protection, while the aluminum core contributes to weight reduction and cost savings. This synergy positions Cu/Al composites as potential replacements for monolithic copper in several industrial domains, most notably in high-current busbars, connectors, heat sinks, and electrical conductors used in electric vehicles and power electronics [9–11].

To overcome the challenges associated with oxide formation, high-temperature oxygen-free rolling (HTOR) has recently gained attention as an effective and scalable approach for fabricating dissimilar metal composites. In the HTOR process, Cu–Al stacks are preheated in a sealed chamber under a controlled non-oxidizing atmosphere, typically a mixture of inert (N_2 or Ar) and reducing (H_2) gases. This environment prevents or removes surface oxides, allowing intimate metallic contact. Rolling at elevated temperatures (400-500 °C) further enhances atomic mobility and promotes solid-state diffusion, enabling the onset of metallurgical bonding during deformation [12–14]. Compared to conventional hot rolling in air, HTOR produces interfaces with fewer voids, thinner oxide residues, and more continuous IMC layers, significantly improving interfacial shear strength and electrical continuity. Beyond oxide suppression, the combination of elevated temperature and controlled deformation in HTOR also modifies grain structures and dislocation distributions, affecting diffusion kinetics during subsequent thermal treatments. Fine-grained or highly deformed zones near the interface can enhance diffusion pathways via increased grain boundary area. This procedure speeds up the development of IMC during annealing. Consequently, understanding how HTOR parameters, such as rolling reduction, pass number, and temperature, affect the pre-annealed interface has become a key step in optimizing post-processing schedules [15–18]. Although HTOR provides a strong foundation for metallurgical bonding, the microstructure of as-rolled Cu/Al composites typically contains high dislocation densities and heterogeneous IMC formation. Hence, subsequent annealing becomes vital to balance strength and ductility while stabilizing the interface.

 doi:10.20944/preprints202601.0095.v1

Annealing facilitates recovery and recrystallization within both Cu and Al layers, releasing internal stresses and restoring ductility. Simultaneously, it promotes further diffusion across the Cu–Al interface, allowing IMC growth and homogenization. However, the annealing process introduces a delicate trade-off [19,20]. Moderate annealing enhances bond strength and toughness through improved diffusion and stress relief. Excessive annealing, by contrast, leads to uncontrolled IMC thickening, particularly the growth of AlCu and Al_4Cu_9 phases, which are highly brittle and prone to cracking under mechanical loading [21,22]. The kinetics of these interfacial reactions typically follow parabolic rate laws governed by diffusion coefficients that vary exponentially with temperature. This highlights the importance of precise control of thermal exposure [23–25]. The optimal annealing parameters are not universal but are influenced by the initial interfacial condition created during rolling, especially the density of defects, interfacial roughness, and proportion of residual oxides. Studies have shown that Cu/Al composites subjected to lower rolling reductions or fewer passes develop thinner, less uniform IMC layers upon annealing due to limited atomic contact. Instead, excessive deformation can introduce cracks or delamination that persist even after diffusion bonding [26–30]. Hence, integrated control of both deformation and heat treatment stages is essential for achieving reliable mechanical properties.

Most prior investigations have focused on bilayer Cu/Al composites, where copper and aluminum are bonded in a two-layer configuration. While these systems are conceptually simpler and easier to fabricate, they exhibit asymmetric mechanical behavior during bending or forming, resulting in uneven stress distributions and interface delamination [31–34]. To mitigate these effects, trilayer Cu/Al/Cu configurations have gained attention in recent years [35–37]. By sandwiching aluminum between two copper layers, the architecture provides mechanical symmetry and improved resistance to flexural stresses. Furthermore, double interfaces can distribute strain more evenly and enhance crack arrest capability during deformation or fatigue loading [38–40]. Beyond its mechanical advantages, the trilayer structure also offers functional benefits. The outer copper layers ensure superior surface conductivity and wear resistance, while the aluminum core significantly reduces mass. Such composites find potential applications in high-current connectors, clad strips, and conductor laminates used in EV power systems and aerospace electrical harnesses [11,41]. Yet, despite their technological promise, systematic studies on the combined effects of rolling and annealing on the interfacial and mechanical evolution of Cu/Al/Cu trilayers remain limited, especially when incorporating high-strength copper alloys rather than pure copper [12].

Recent advances in alloy design have introduced precipitation-strengthened copper alloys, such as Cu18150 (Cu–Cr–Zr), as candidate materials for demanding electrical and mechanical applications. The alloy derives its strength from fine Cr and Zr precipitates, which impede dislocation motion and provide superior thermal stability compared to pure copper. Its high conductivity (≈80-90% IACS), combined with exceptional hardness and wear resistance, makes it ideal for high-load electrical contacts and electrodes [42,43]. When integrated into a composite system with aluminum, Cu18150 significantly influences interfacial diffusion kinetics due to solute drag effects and modified grain boundary behaviors. The diffusion of alloying elements (Cr, Zr) may also alter IMC nucleation or growth, potentially stabilizing desirable interfacial morphologies [17,22,42]. However, despite these advantages, substantial unexplored questions remain regarding Cu–Cr–Zr/Al interfaces. Most prior works on Cu/Al thermomechanical processing have used high-purity copper, neglecting the compositional complexity introduced by alloying elements. The possible partitioning of Cr or Zr at the interface, their effect on IMC phase selection, and their impact on mechanical response under tensile loading or fracture conditions remain poorly understood. Addressing these questions is vital for designing robust Cu–Al multilayer composites compatible with modern electrical and structural demands [44–46].

The manufacturing sequence of HTOR followed by controlled annealing introduces a coupled thermomechanical system, where each stage strongly influences the other. The rolling process establishes the initial defect density, interfacial roughness, and bonding integrity, all of which define the subsequent diffusion behavior during annealing. Inadequate deformation limits atomic contact,

 doi:10.20944/preprints202601.0095.v1

leading to discontinuous diffusion fronts; excessive deformation generates micro-cracks and localized heating, resulting in distorted diffusion pathways and potential IMC discontinuities. Therefore, determining the optimal rolling reduction and pass number is crucial to forming a uniform, defect-minimized interface that can evolve favorably during heat treatment [26,30,34,47]. Equally critical is the annealing temperature and time combination, which governs IMC thickening rate, recrystallization extent, and stress relaxation. At lower annealing temperatures (≈300 °C), recovery and limited diffusion occur, improving ductility without substantial IMC growth. When temperatures approach 450 °C, recrystallization accelerates and diffusion becomes dominant, forming thicker IMC layers (Al_2Cu and AlCu). These IMC layers, beyond an optimal thickness (typically 1-3 μm), may act as crack initiation sites during tensile loading [21,48–51]. Elucidating how these microstructural factors interact to determine mechanical properties, particularly the trade-off between strength and ductility, is a necessary step toward process optimization.

The mechanical performance of Cu/Al multilayer composites is fundamentally linked to the nature of their interfaces. Unlike monolithic metals, fracture in layered composites is typically interface-controlled. The transition between ductile and brittle behavior depends on IMC thickness, bonding continuity, and the residual stress state near the interface [52–54]. Thin IMC layers (<2 μm) tend to deform coherently with the base metals, enhancing tensile strength through effective load transfer. Once the layer becomes excessively thick (>5 μm), brittle intergranular fracture along IMCs dominates, drastically reducing elongation and toughness [23,55–57]. Tailored post-rolling annealing can thus be viewed as a mechanical optimization strategy, not merely a thermal relaxation step. High bonding strength and sufficient ductility can be attained through precise control of diffusion kinetics, grain recovery, and interface chemistry. Quantitative correlations between microstructural evolution (IMC morphology, grain size distribution, dislocation density) and macroscopic mechanical responses (yield strength, ultimate tensile strength, elongation) provide a pathway to designing process–structure–property relationships essential for industrial application [21,48,58].

Despite extensive studies on Cu/Al bonding mechanisms, several key gaps remain in the current body of knowledge. (i) Trilayer composite systems: Research has largely concentrated on bilayer Cu/Al systems, neglecting the mechanical symmetry and improved stress distribution achievable in trilayer designs. Also, the dynamic interplay between dual interfaces during rolling and annealing, including diffusion asymmetry and composite bending performance, remains underexplored [30,59]. (ii) Influence of alloyed copper: The introduction of alloying elements such as Cr and Zr in copper adds another dimension to interfacial diffusion kinetics and phase stability. Their potential to modify IMC formation, interface adhesion, or fracture pathways is poorly documented in the current literature [45,60]. (iii) Coupled effects of rolling and annealing: Existing studies typically examine rolling and annealing in isolation. A holistic understanding of how rolling-induced microstructural states (defects, texture, dislocation density) affect subsequent annealing kinetics, and consequently mechanical properties, remains lacking [21,30,34]. Addressing these gaps is essential for developing a unified processing framework that links rolling parameters, annealing conditions, and interfacial microstructure to optimize mechanical performance.

The present research aims to systematically investigate the interfacial design and mechanical optimization of Cu–Al–Cu trilayer composites fabricated through HTOR, followed by tailored annealing treatments. The specific focus lies in understanding how the synergy between deformation-induced structures and diffusion-driven transformations dictates interfacial evolution and composite properties. The study employs Cu18150 (Cu–Cr–Zr alloy) as the outer layers and Al1060 as the core to explore the following objectives: (i) To fabricate Cu18150Cu/Al1060/Cu18150Cu trilayer composites using HTOR under various rolling passes (1-4) and quantify how deformation influences the initial bonding condition. (ii) To systematically investigate annealing parameters, temperature (300-450 °C) and duration (0.5-2 h), to determine their effects on IMC growth, microstructural uniformity, and interfacial integrity. (iii) To correlate microstructural evolution with mechanical performance, particularly tensile strength, ductility, and fracture morphology, enabling the establishment of structure–property relationships. (iv) To identify diffusion mechanisms (grain

 doi:10.20944/preprints202601.0095.v1

boundary vs. lattice diffusion) governing IMC evolution through kinetic modeling and microanalysis. (v) To propose optimized processing parameters that deliver a balanced combination of strength and ductility suited for structural and functional applications of Cu–Al multilayer composites.

By integrating process control, interfacial characterization, and mechanical evaluation, this study aims to contribute to the fundamental understanding of Cu–Al composite metallurgy while offering practical guidelines for industrial manufacturing. Beyond the immediate application in power and transportation systems, insights from this research could extend to other dissimilar metal systems where interface control is critical, such as Cu–Ni, Cu–Mg, or Al–Fe multilayers used in advanced conductors and lightweight hybrid components [61,62]. The broader significance lies in demonstrating how thermomechanical coupling via rolling-induced microstructural tailoring followed by diffusion-managed annealing can serve as a rational design framework for next-generation metal–metal composites. As industries advance toward electrification and sustainable performance optimization, such materials are poised to play a pivotal role in future engineering systems where multifunctional performance, manufacturability, and reliability converge.

2. Materials and Methods

2.1. Materials

Commercially sourced base materials were employed in this study. The outer layers were made of copper-chromium-zirconium alloy (Cu18150) sheets, conforming to ASTM B631 standards for precipitation-hardenable copper alloys. Their chemical composition was quantitatively verified via optical emission spectroscopy (OES) using a Skyray OES8000 spectrometer (Jiangsu Skyray Instrument Co., Ltd., Kunshan, China), equipped with a high-performance linear array CCD detector and Paschen-Runge polychromator. Analysis was conducted under argon atmosphere with digital plasma spark excitation (100-1000 Hz frequency, 1-60 A current, and high-energy pre-spark mode), following surface preparation by mechanical grinding and turning to ensure flat, contaminant-free analytical areas. Calibration utilized certified reference materials (CRMs) traceable to GBW standards for Cu-Cr-Zr matrices, achieving detection limits below 10 ppm for key alloying elements. Triplicate measurements yielded results with <1% relative standard deviation, as detailed in Table 1. This alloy's strength derives from fine, coherent Cr_2Zr precipitates formed during aging, which effectively impede dislocation motion while preserving high electrical conductivity.

Table 1. Chemical composition of the 18150 copper alloy and 1060 aluminum alloys in wt.% [63].

	Cu	Cr	Zr	Zn	Al	Fe	Si	Ni	Mn	Mg
Cu18150	99.081	0.720	0.102	0.042	0.023	-	0.0079	0.015	0.0006	0.0004
Al1060	0.050	0.0008	-	0.039	98.9	0.50	0.460	0.0037	0.0041	0.0033

2.2. Composite Fabrication via High-Temperature Oxygen-Free Rolling

The Cu18150/Al1060/Cu18150 trilayer composites were fabricated through a three-stage high-temperature oxygen-free rolling (HTOR) process, designed to ensure oxide-free metallurgical bonding while controlling the evolution of interfacial microstructure. Commercially sourced Cu18150 alloy sheets (initial thickness: 2.0±0.05 mm; purchased from Shanghai Unique Alloy Co. Ltd., Shanghai, China) and AA1060 aluminum sheets (initial thickness: 3.0±0.05 mm; purchased from Jiangsu Skyray Instrument Co., Ltd.) were precision-cut to dimensions of 100 mm × 50 mm using a waterjet cutter to minimize edge contamination. Bonding surfaces were sequentially ground with 400-, 600-, and 800-grit SiC abrasive papers to remove native oxide layers, achieving a centerline average roughness (Ra) of <0.4 μm as verified by profilometry. Surfaces were then degreased via ultrasonic cleaning in acetone (5 min) followed by absolute ethanol (3 min), and dried with compressed argon to prevent reoxidation.

 doi:10.20944/preprints202601.0095.v1

A symmetric Cu18150/Al1060/Cu18150 sandwich stack was assembled with precise alignment under optical microscopy to ensure uniform contact between layers. The assembly was promptly loaded into a custom-fabricated, vacuum-sealed quartz retort furnace (Beijing GF Co., Ltd., Beijing, China; maximum temperature of 1200°C, vacuum capability of 10^{-3} Pa) directly coupled to the rolling mill via a heat-insulated transfer trolley (transit time: <10 s). The chamber was evacuated to 10^{-2} Pa, then backfilled and purged three times with ultrahigh-purity argon, establishing a reducing atmosphere of 95 vol.% N_2 + 5 vol.% H_2. The stack was ramped to 500±5 °C at 10 °C/min and soaked for 30 min, promoting surface activation via H_2-mediated oxide dissociation while ensuring through-thickness thermal homogeneity (gradient <5 °C, monitored by three K-type thermocouples).

Hot rolling was performed on a laboratory-scale two-high reversing rolling mill (Jiangsu Guangduan Machinery Co., Ltd., Wuxi, China; roll diameter of 300 mm, barrel width of 200 mm, maximum separating force of 500 kN). Preheated stacks were transferred within 8-10 s and rolled unlubricated (dry rolls, μ≈0.3-0.4) to maximize shear-driven atomic mixing at interfaces. Progressive reductions were applied in four passes at an inter-pass temperature of 450-480 °C (measured via infrared pyrometer): Pass 1: 35% reduction (to 3.9 mm), Pass 2: 38% (to 2.4 mm), Pass 3: 33% (to 1.6 mm), and Pass 4: 44% (to 0.9±0.02 mm final thickness), yielding cumulative ~70% deformation. Roll speed was maintained at 0.1-0.15 m/s (20-30 rpm), with ~20-30 s inter-pass equilibration in the retort. Post-final pass, samples were air-cooled to room temperature (~25 °C) at 15 °C/min in ambient air. This integrated HTOR sequence, high-temperature deformation under inert/reducing conditions, effectively suppressed oxide entrapment while tailoring defect densities for controlled post-rolling annealing responses.

2.3. Post-Rolling Heat Treatment (Annealing)

Systematic post-rolling annealing treatments were employed to influence the evolution of IMCs, alleviate residual stresses caused by deformation, and enhance the balance between strength and ductility in the Cu18150/Al/Cu18150 trilayer composites. All annealing experiments were conducted in an NBD-M1200-30IT high-temperature box furnace (NBD Material Technology Co., Ltd., Nanjing, China; maximum temperature: 1200 °C), featuring silicon carbide heating elements, K-type thermocouple control (±1 °C accuracy), and a 16-segment programmable PID temperature controller. To mitigate surface oxidation during air exposure, samples were precision-wrapped in type 304 stainless steel foil pouches (0.05 mm thick, seam-sealed under argon flush) before insertion. The systematic annealing protocol comprised three sequential phases, as outlined below.

- **Phase 1:** Temperature screening. Representative samples from each of the four rolling passes (final thicknesses: 3.9, 2.4, 1.6, 0.9 mm) underwent broad temperature exploration at 300, 350, 400, and 450 °C, each with a 2 h isothermal hold. This phase established preliminary IMC growth kinetics and recovery/recrystallization thresholds, with furnace cooling (~3 °C/min) to ambient temperature (~ 25 °C).
- **Phase 2:** Temperature refinement. Informed by Phase 1 outcomes, a narrower matrix of 360, 380, 400, 420, and 450 °C was applied to the most promising rolling condition (Pass 4, 70% cumulative reduction), using a standardized 1 h hold time. This refinement targeted the optimal window for balanced IMC thickening (1-3 μm) while preserving matrix ductility. Phase 3: Time optimization. Building on the identified optimal temperature from Phase 2, dwell times of 0.5, 1.0, 1.5, and 2.0 h were evaluated for the selected rolling-annealing combination. This phase quantified time-dependent diffusion and phase stability.

Across all phases, samples were ramped from room temperature to target values at a controlled rate of 10±1 °C/min, with overshoot limited to <5 °C via the furnace's adaptive control algorithm. Post-annealing, foil-wrapped specimens were transferred to a desiccator within 30 s to prevent moisture ingress, ensuring microstructural fidelity for subsequent characterization. Temperature profiles were continuously logged at 1 s intervals using the furnace's integrated data acquisition system, with independent verification via embedded K-type thermocouples. This multi-phase

 doi:10.20944/preprints202601.0095.v1

strategy enabled the construction of comprehensive process–microstructure–property maps for HTOR-annealed Cu18150/Al1060/Cu18150 systems.

2.4. Microstructural Characterization

Cross-sectional specimens for microstructural examination were extracted perpendicular to the rolling direction (RD) using a precision slow-speed diamond saw to minimize heat-affected zones and edge artifacts. Samples were hot-mounted in phenolic conductive resin to ensure edge retention and electrical grounding. Progressive mechanical preparation followed metallographic standards: grinding with P400, P800, P1200, and P2000 SiC papers (under ethanol lubrication, 150-300 rpm wheel speed), followed by diamond polishing (9, 6, and 3 μm suspensions on automated platen). Final surface finishing employed 1 μm alumina suspension and vibratory polishing with 0.05 μm colloidal silica to achieve mirror-like surfaces without relief polishing artifacts. No chemical etching was required, as backscattered electron (BSE) contrast inherently delineated phases.

Microstructural analysis and interfacial characterization were conducted using a Phenom XL G2 Desktop Scanning Electron Microscope (Thermo Fisher Scientific, distributed by Phenom Scientific Instrument (Shanghai) Co., Ltd., Shanghai, China) operating at 15 kV accelerating voltage, ~10 mm working distance, and 30° sample tilt for optimal interface resolution. The system featured a CeB_6 electron source, backscattered electron (BSE) detector, and integrated Energy Dispersive X-ray Spectroscopy (EDS). BSE imaging exploited Z-contrast to clearly resolve Cu18150 layers (bright), Al1060 core (dark), and IMCs (intermediate gray: Al_2Cu, AlCu). Interfacial IMC thickness was quantified at 25 equidistant locations per sample (500 nm spacing) using ImageJ/FIJI v1.54f, reporting mean ± standard deviation (σ). Elemental mapping (Al K_α, Cu L_α, O K_α, Cr K_α, Zr L_α; 1024×768 px, 100 μs dwell/pixel, 5 min acquisition) and point analyses elucidated diffusion profiles, phase identification (via Cu/Al ratios), and microsegregation.

2.5. Mechanical Testing

Tensile specimens conformed to ASTM E8/E8M sub-size flat geometry (Type 1A sheet specimen, scaled): gauge length 25 mm, width 6 mm, total length 100 mm, fillet radius 6 mm, with loading axis parallel to RD. Electrical discharge machining (EDM, wire diameter 0.25 mm, spark energy 0.5 mJ) ensured precise geometry and damage-free surfaces, verified by optical profilometry. The full composite thickness (0.9-3.9 mm) was retained as-received. Quasi-static tensile tests were executed at 23±2 °C using a WDW-10S electromechanical universal testing machine (Jinan Hensgrand Instrument Co., Ltd., Jinan, China). A constant crosshead displacement rate of 1.0 mm/min yielded an initial engineering strain rate of 6.7×10^{-4} s^{-1}. Strain measurement employed a non-contact video extensometer (integrated ARAMIS system, 12 MP camera, 25 Hz acquisition, 0.05% strain resolution) tracking two 6×6 mm speckle-patterned regions on the gauge, eliminating grip effects and enabling full stress-strain curves to fracture. Load signals were acquired at 100 Hz via a 24-bit ADC. Minimum n=5 valid replicates per condition ensured statistical robustness (rejection criterion: >10% deviation from mean). Engineering stress-strain data yielded yield strength, ultimate tensile strength, uniform elongation, and total elongation. Fractography utilized the aforementioned Phenom XL G2 SEM at 5–20 kV to document failure modes: ductile dimpling (Al matrix), transgranular cleavage (Cu/IMCs), intergranular decohesion, and interfacial delamination. Cross-sectional failure analysis correlated crack paths with IMC morphology and residual stresses. All data satisfied ISO 6892-1 Class B1 precision requirements.

 doi:10.20944/preprints202601.0095.v1

3. Results and Discussion

3.1. Evolution of Interfacial Microstructure

3.1.1. Effect of Rolling Pass Number

Initial bonding was achieved via high-temperature oxygen-free rolling. The interfacial morphology was strongly dependent on the number of rolling passes. After a single pass, the Cu/Al interface exhibited a pronounced wavy, non-uniform contour (Figure 1a), indicative of deformation incompatibility between the dissimilar metals. At this stage, IMCs were present but discontinuous along the interface, with varying layers (1-3 layers). This observation supports the notion of non-uniform atomic diffusion occurring in the system. In this regard, the EDS point analysis (Table 1) identified three distinct IMCs of Al_2Cu adjacent to the Al layer, AlCu in the middle, and Al_4Cu_9 adjacent to the Cu layer. The total IMC layer thickness was approximately 2 μm. EDS mapping (Figure 1e-f) revealed sharp elemental boundaries, confirming that bonding was predominantly mechanical with limited diffusion. With an increasing number of rolling passes (2 to 4), the interfacial waviness was progressively reduced, achieving a near-flat interface after four passes (Figure 1b-d). The IMC layer became more uniform, consistently presenting a three-layer structure; however, its continuity along the interface decreased with increasing passes. Crucially, the total IMC thickness remained largely unaffected by the number of passes, with variations of less than 1 μm. This suggests that rolling deformation primarily influences interfacial conformity and defect density, rather than the extent of diffusion-driven growth during the brief high-temperature rolling contact.

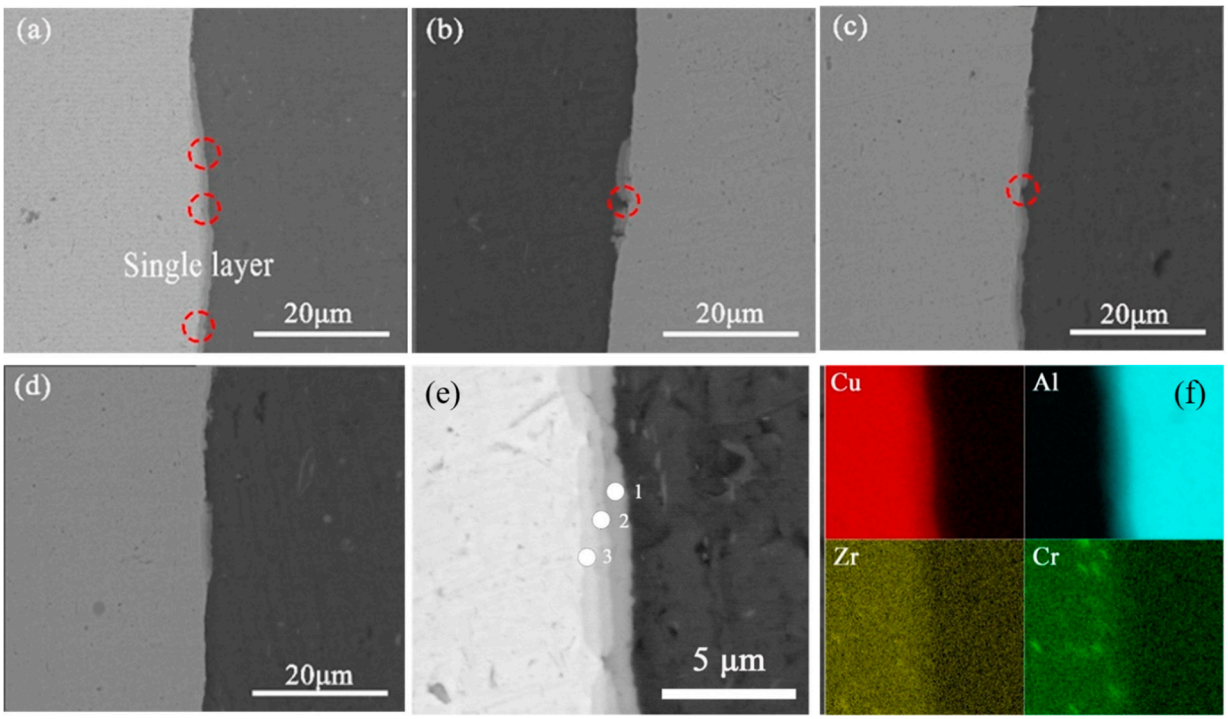

Figure 1. SEM observation of as-rolled interfaces showing the effect of rolling passes of (a) 1 pass, (b) 2 passes, (c) 3 passes, (d) 4 passes, (e-f) EDS elemental mapping of 1-pass-processed sample indicating the distributions of Cu, Al, Zr, and Cr at the interface.

The pronounced wavy interface observed after a single rolling pass reflects the inherent deformation incompatibility between Cu18150 and Al1060 layers during HTOR. This situation arises from differential flow stresses leading to interfacial buckling and mechanical interlocking rather than uniform metallurgical bonding [64]. The observed topography, along with the presence of discontinuous IMCs that display a variable three-layer structure (Al_2Cu, AlCu, and Al_4Cu_9),

 doi:10.20944/preprints202601.0095.v1

highlights that the initial diffusion process is quite localized. This phenomenon is influenced by short thermal exposure and the atomic mixing that occurs at asperity contacts due to shear forces. This is further supported by the sharp elemental gradients revealed through EDS analysis, which primarily suggest mechanical adhesion with limited solid-state intermixing. The progressive increase in rolling passes, up to four, systematically flattens the interface by improving layer conformity and distributing deformation more homogeneously. However, the continuity of IMC decreases, even though the total thickness remains consistent at around 2 μm. This suggests that the number of passes mainly influences defect density and topography, rather than cumulative diffusion, as the rolling dwell times are still limited by interface reactions [65]. This pass-dependent interfacial evolution aligns with established deformation-diffusion coupling in dissimilar metal cladding. While low passes preserve high surface area for subsequent diffusion but introduce stress concentrators. In contrast, high passes promote flatness at the cost of reduced atomic contact sites, influencing post-rolling annealing responses.

Table 1. Point analysis composition of 1-pass-processed sample.

Spot	Element	Atomic Concentration	Components
1	Al	62.09	Al_2Cu
	Cu	37.91	
2	Al	47.64	AlCu
	Cu	52.36	
3	Al	37.85	Al_4Cu_9
	Cu	62.15	

3.1.2. Effect of Post-Rolled Annealing Temperature

Subsequent annealing profoundly transformed the interfacial microstructure from mechanical to metallurgical bonding. For samples annealed at 400 °C for 2 hours (Figure 2A), the IMC layer thickened significantly, became continuous, and displayed a uniform three-layer structure across all rolling passes. The initial waviness from rolling was preserved, but the IMC layers now grew uniformly perpendicular to the interface. A systematic investigation of annealing temperature revealed a strong thermally activated growth behavior. As shown in Figures 2B and 3, IMC thickness increased dramatically with temperature: from ~2 μm (as-rolled) to ~4 μm (350 °C/2 h), ~10 μm (400 °C/2 h), and ~18 μm (450 °C/2 h). Furthermore, the growth kinetics of the individual IMC layers were temperature-dependent. At lower temperatures (≤400 °C), the Al_2Cu layer (Al-side) grew at a higher rate. At 450 °C, the growth rate of the Cu-side Al_4Cu_9 layer surpassed that of Al_2Cu, resulting in a thicker Al_4Cu_9 layer after 2 hours.

 doi:10.20944/preprints202601.0095.v1

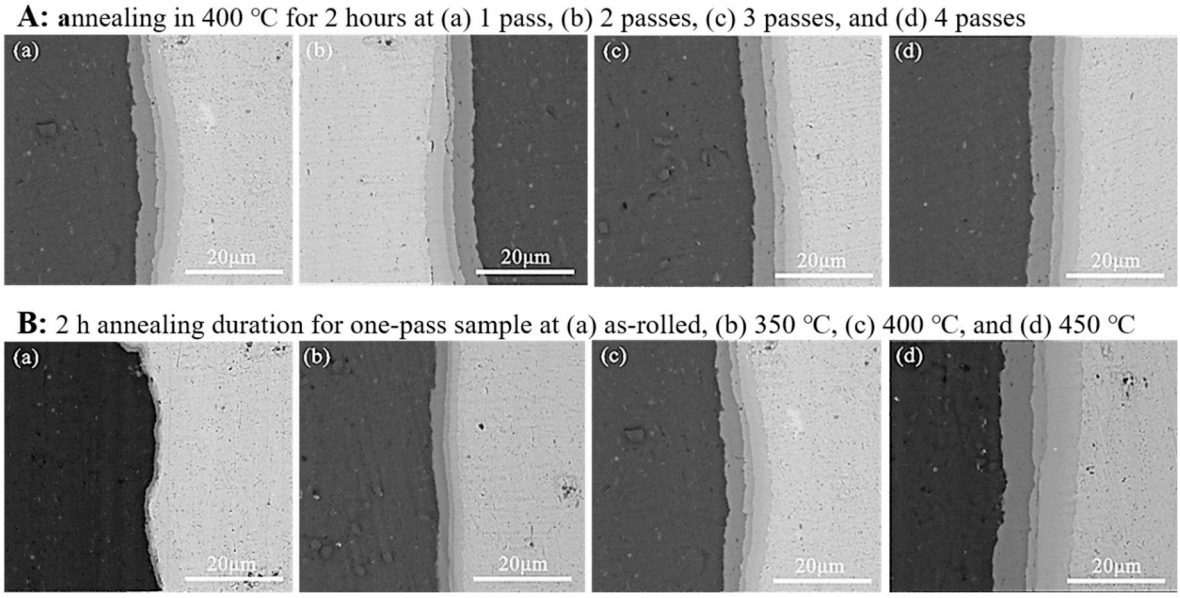

Figure 2. SEM observation of samples at different pass numbers of 1, 2, 3, and 4 and at temperatures of 350, 400, and 450 °C.

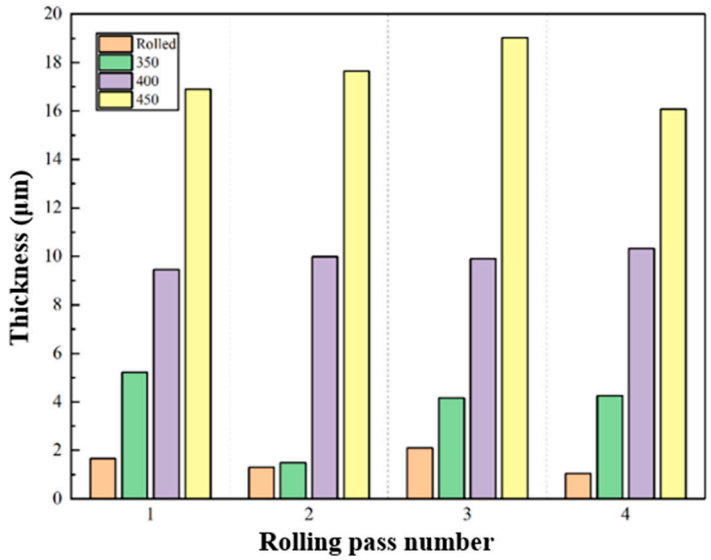

Figure 3. Thickness of the interfacial compound layer in the as-rolled state and the annealed conditions after holding at different temperatures of 350, 400, and 450 °C for 2 hours under different rolling pass numbers of 1, 2, 3, and 4.

The growth kinetics were quantitatively analyzed using the parabolic growth law, $x^2=kt$, where the rate constant k follows an Arrhenius relationship, $k=k_0exp(-Q/RT)$. A modified equation, $(x_t-x_0)^2=kt$, accounted for the initial IMC layer thickness (x_0) from rolling. Excellent linear fits of lnk versus $1/T$ were obtained for both 1-hour and 2-hour annealing series (Figure 4a and 4b). The calculated apparent activation energy Q was approximately 138.1 kJ/mol for 1-hour annealing and 121.5 kJ/mol for 2-hour annealing conditions. The higher Q and pre-exponential factor k_0 associated with shorter annealing times indicate a transition in the dominant diffusion mechanism. Initially, defect-assisted diffusion, such as pipe diffusion along dislocations and grain boundaries, plays a crucial role in the initial and rapid growth phases. In contrast, bulk lattice diffusion dominates the later steady-state growth phase [66].

 doi:10.20944/preprints202601.0095.v1

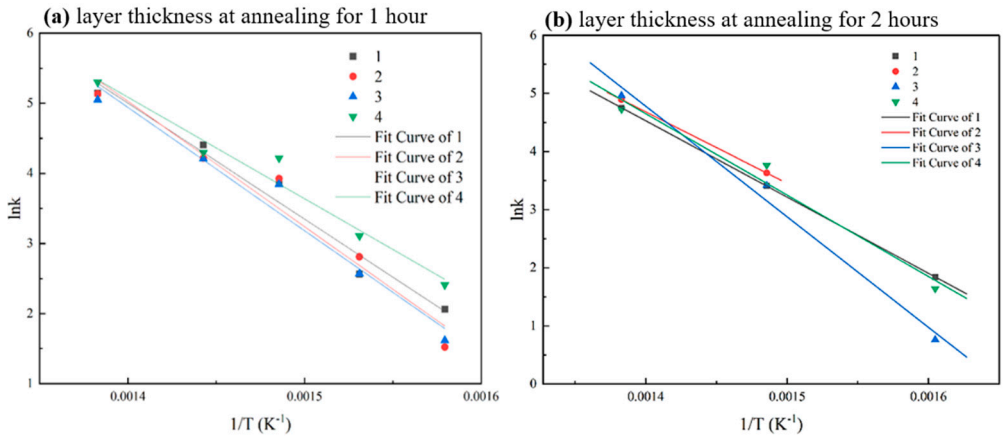

Figure 4. Fitting curves of the interface compound layer thickness at annealing temperatures of (a) 1 hour, (b) 2 hours.

Annealing at 400 °C for 2 hours transforms the as-rolled mechanical interface into a continuous, uniform three-layer IMC structure across all pass conditions. This process maintains the waviness that allows for perpendicular growth. Additionally, elevated temperatures ranging from 350 to 450 °C lead to exponential thickening from approximately 2 μm to 18 μm, through thermally activated diffusion. As the temperature rises, the composition of IMCs shifts from Al_2Cu at temperatures up to 400 °C to Al_4Cu_9 at 450 °C, due to growth kinetics that favor copper-side diffusion at higher homologues [27].

Parabolic growth analysis, taking into consideration the initial IMC (x_0), reveals Arrhenius-derived activation energies of 138.1 kJ/mol (1 h) and 121.5 kJ/mol (2 h). The observed elevated short-time Q values suggest the presence of defect-pipe diffusion pathways, which are introduced by rolling-induced dislocations. As these defects anneal out, the process transitions to lattice diffusion. This behavior aligns with existing literature on Cu-Al systems, where Q~120-140 kJ/mol signals grain boundary/pipe mechanisms [66]. The findings highlight temperature as the key factor influencing kinetics. Optimal regimes (≤400 °C) produce thin, ductile IMCs that improve bond strength without causing embrittlement. However, at 450 °C, excessive thickening occurs, leading to the formation of brittle Al_4Cu_9, which aligns with previous reports on the importance of IMCs in clad composites.

3.1.3. Effect of Post-Rolled Annealing Duration

The time-dependent evolution of the IMC layer at 400 °C exhibited a non-monotonic trend (Figure 5a-e). After 0.5 hours, the layer reached ~11.5 μm. Unexpectedly, the thickness decreased to ~10.4 μm after 1 hour before increasing again to ~14.0 μm after 2 hours. This thickness reduction between 0.5 h and 1 h is attributed to an interfacial densification process. The initial, defect-assisted rapid growth likely produces a porous or structurally deficient IMC layer. With extended annealing, atomic rearrangement and healing of micro-voids lead to a denser, more stable interface, manifesting as a slight reduction in the measured thickness. Subsequent growth follows the classical parabolic law, as confirmed by the linear fit of x^2 versus t for data from 1 to 2 hours.

 doi:10.20944/preprints202601.0095.v1

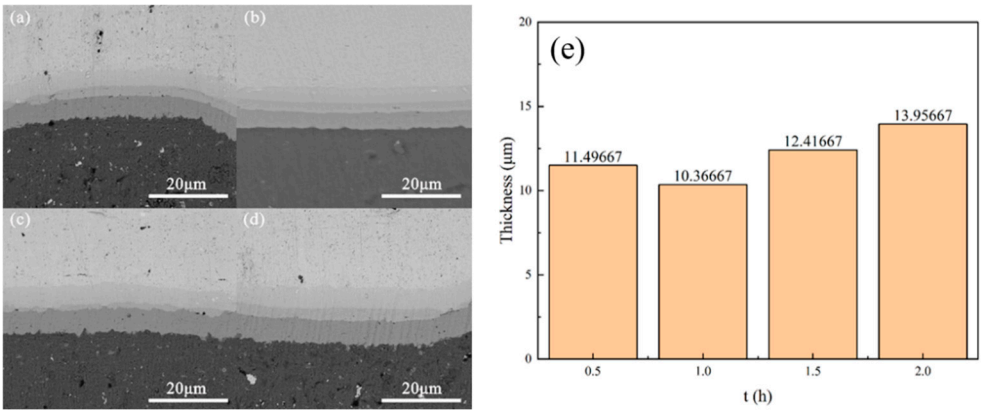

Figure 5. SEM observation of 1-pass-processed sample annealed at 420 ℃ for different duration times of (a) 0.5 h, (b) 1 h, (c) 1.5 h, and (d) 2 h; (e) thickness of interfacial compound layer of 1-pass-processed sample annealed at 420 ℃ for different duration times of 0.5 h, 1 h, 1.5 h, and 2 h.

At 400 °C, the evolution of IMC shows a complex behavior that deviates from simple parabolic kinetics. Initially, there is a rapid increase in thickness to approximately 11.5 μm within the first half hour, driven by defect-assisted diffusion that leads to the formation of porous structures. This is followed by a densification process, resulting in a thickness of about 10.4 μm after one hour, which occurs through the annihilation of vacancies and rearrangement of atoms. After this stage, the growth pattern shifts to a parabolic regrowth, reaching around 14.0 μm by the two-hour annealing, as confirmed by linear fits of x◎ versus time after densification. The transient thinning reflects microstructural stabilization. Here, the excess vacancies and dislocations inherited from the rolling process initially promote rapid growth. However, during extended holds, these structures settle into more stable and equilibrium configurations, which helps to avoid the Kirkendall voiding often seen in prolonged Cu-Al diffusion couples [30]. Such behavior underscores the importance of annealing time in striking a balance between the completeness of diffusion and the stability of phases. Achieving optimal uniformity at 1 hour minimizes defects while preventing the excessive growth of brittle phases, aligning with kinetic models that focus on the thresholds for defect annihilation in deformed interfaces.

3.2. Evolution of Mechanical Properties

3.2.1. Effect of Rolling Pass Number

In the as-rolled state, the material exhibited classic work-hardening behavior (Figure 6A). The ultimate tensile strength (UTS) increased from 250 MPa (1 pass) to 344 MPa (4 passes). Conversely, elongation (EL) drastically decreased from 18.3% to 1.2%. The stress-strain curves for low-pass samples showed serrations, indicating interfacial delamination and poor bond strength. High-pass samples displayed smooth curves, suggesting improved interfacial integrity and cooperative deformation. Annealing altered this relationship (Figure 6B). For single-pass material, annealing maintained UTS near 250 MPa while dramatically improving EL to over 20% (peaking at 25.8% at 400 °C/2h), as work hardening was relieved and metallurgical bonding was achieved. For multi-pass materials, annealing significantly reduced UTS (e.g., from 344 MPa to ~200 MPa for 4 passes) due to the elimination of work hardening, but improved EL compared to the brittle as-rolled state. The optimal combination of strength and ductility after annealing was consistently found in the single-pass material, benefiting from its lower initial dislocation density and sufficient interfacial development upon annealing.

 doi:10.20944/preprints202601.0095.v1

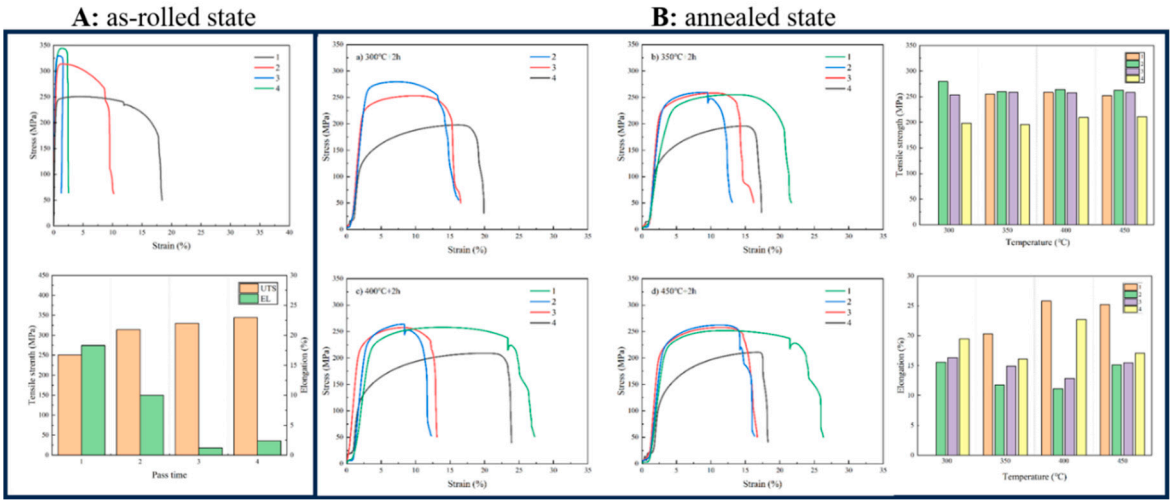

Figure 6. A: Effect of different rolling pass numbers on stress-strain curves and tensile strength in the as-rolled state, and B: Stress-strain curves, tensile strength, and elongation of different rolling pass numbers under different annealing temperatures with a 2-hour holding time.

The tensile response of as-rolled materials highlights the significant role of work-hardening, as evidenced by the increase in ultimate tensile strength from 250 MPa after one pass to 344 MPa after four passes. This improvement is attributed to the rising dislocation densities. However, there is a catastrophic reduction in ductility, which drops from 18.3% to 1.2%. This loss is linked to strain localization and delamination observed in the low-pass serrated curves, which then shift to a smoother cooperative deformation in the higher passes due to improved conformity. After the annealing process, single-pass materials retain UTS (~250 MPa) while recovering EL>20% through recovery and metallurgical bonding. In contrast, materials that undergo multiple passes experience a significant decrease in tensile strength, dropping to around 200 MPa due to recrystallization, which negates hardening effects, though EL improves modestly. This observation highlights the advantages of low passes for achieving a favorable balance of properties, utilizing minimal initial hardening to maximize interfacial benefits [64]. The observed trends highlight the role of rolling passes as topography tuners, where low-pass wavy interfaces enable superior annealing-induced strengthening without excessive softening. This aligns with research on deformation preconditioning aimed at achieving the optimal strength-ductility synergy in clad systems.

3.2.2. Effect of Post-Rolled Annealing Temperature

The influence of annealing temperature on UTS followed a parabolic trend. For 2-hour anneals, UTS peaked at 400 °C (~258 MPa for 1 pass) and dropped at 450 °C due to excessive growth of brittle IMCs (Figure 7). For 1-hour anneals with finer temperature intervals, the peak shifted to 420 °C, reaching 258.9 MPa for single-pass material (Figure 8). Ductility response was complex and pass-dependent. Single-pass material showed peak ductility at 400-420 °C. Multi-pass materials, due to the competition between recrystallization (improving ductility) and brittle IMC growth (reducing it), exhibited more variable EL trends. Critically, low-pass materials annealed at high temperatures (450 °C) reverted to delamination failure, as evidenced by serrated stress-strain curves, due to stress concentration at the wavy interface and crack initiation in the thick, brittle AlCu layer.

 doi:10.20944/preprints202601.0095.v1

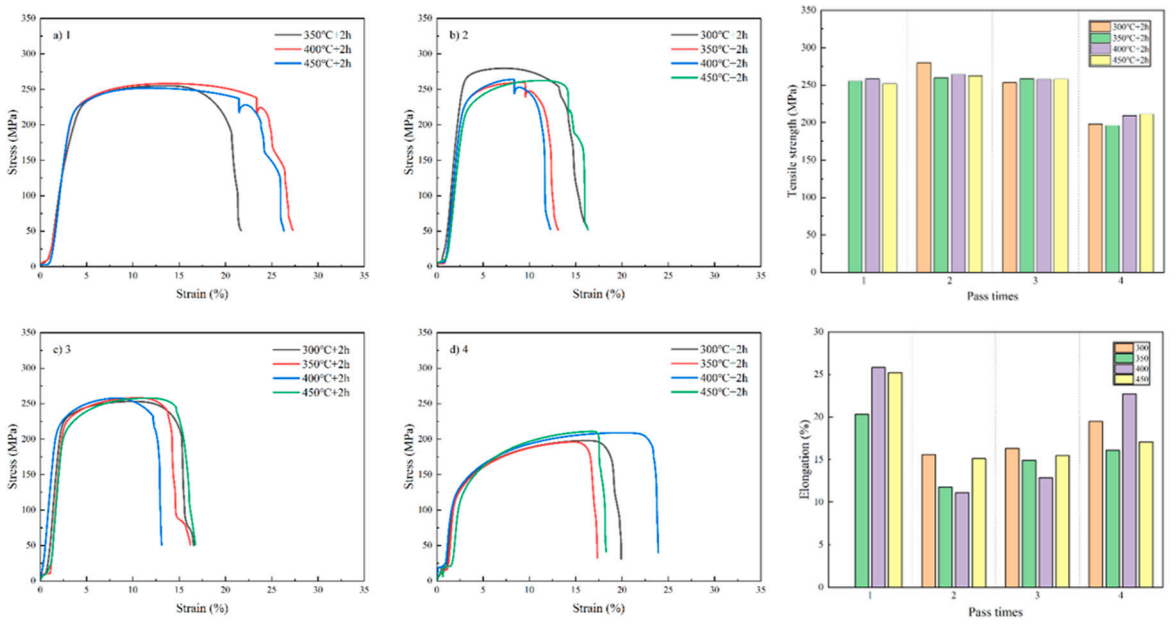

Figure 7. Stress-strain curves, tensile strength, and elongation at different annealing temperatures for a 2-hour duration at various rolling pass numbers.

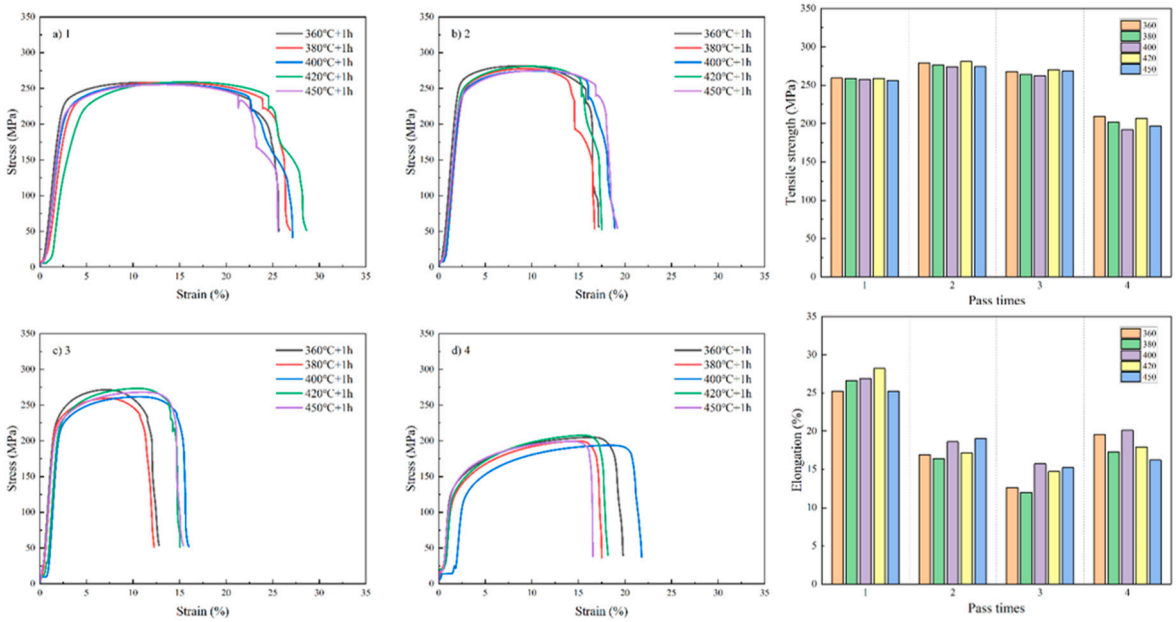

Figure 8. Stress-strain curves, tensile strength, and elongation at different annealing temperatures for a 1-hour duration at various rolling pass numbers.

UTS exhibits a parabolic relationship with temperature, reaching its highest point at approximately 258 MPa when subjected to annealing in 400-420 °C for 1-2 hours. Beyond 450 °C, a decline occurs due to the formation of brittle intermetallic compounds, which leads to delamination, as indicated by serrations in the low-pass curves. In contrast, elongation is optimized in a single pass at 400-420 °C, where a balance between recovery and bonding is achieved. The variability observed in multi-pass processes reflects the competition between recrystallization and embrittlement. Low-pass superiority persists, as they can tolerate moderate intermetallic compounds while also increasing the risk of cracking at high temperatures. In contrast, flat high-pass interfaces manage to distribute stress effectively but are prone to softening of the base metal. This delineates annealing temperature as the arbiter of performance trade-offs, where 400-420 °C windows maximize

 doi:10.20944/preprints202601.0095.v1

load transfer through thin IMCs, corroborated by fracture mechanics models positing optimal IMC thickness ~5–10 μm for peak toughness in Cu-Al laminates [27].

3.2.3. Effect of Post-Rolled Annealing Duration

At the optimal 420 °C, the effect of annealing time on single-pass material was investigated (Figure 9). UTS increased from 257.3 MPa (0.5 h) to a peak of 258.9 MPa (1 h), slightly decreased at 1.5 h (256.3 MPa), and recovered at 2 h. EL peaked at 28.2% after 1 hour and then declined. This non-monotonic behavior correlates directly with the microstructural evolution. The 1-hour condition corresponds to the densified, optimally thick (~10.4 μm), and uniform IMC layer, providing strong bonding without excessive embrittlement. Shorter times yield incomplete bonding, whereas longer periods promote the development of the embrittling AlCu phase. At 420 °C, the single-pass UTS reaches a maximum of 258.9 MPa, while elongation is recorded at 28.2% after 1 hour. This outcome is associated with a densified intermetallic compound measuring approximately 10.4 μm. In contrast, a shorter duration of 0.5 hours results in incomplete bonding, and extending the time beyond 1.5 hours leads to embrittlement due to AlCu. The observed non-monotonic behavior reflects the microstructural densification process, where the 1-hour achieves an equilibrium state without the occurrence of excess diffusion. This condition results in an optimal strength-ductility product, fulfilling the specified targets (≥220 MPa and ≥20% EL). Time optimization thus refines the process envelope, emphasizing the importance of short holds for defect healing without overgrowth. This approach aligns with diffusion couple experiments that support time-temperature-transformation frameworks for IMC control [30].

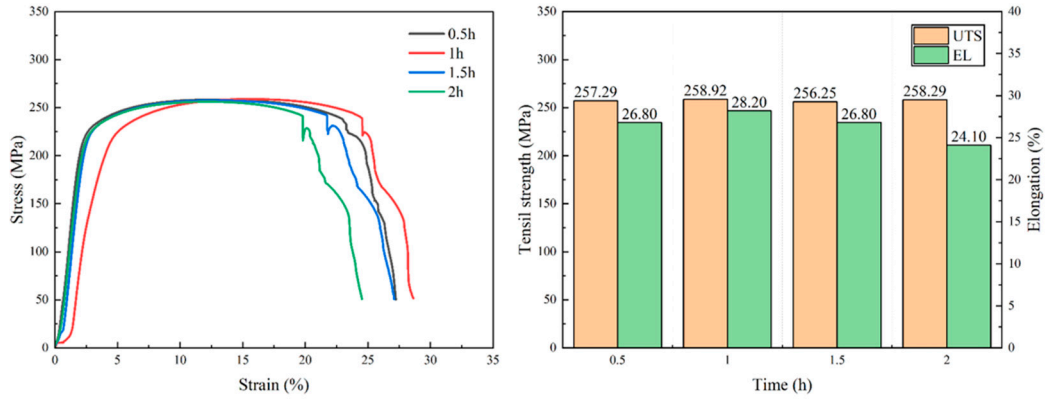

Figure 9. Stress-strain curves, tensile strength, and elongation of annealing at 420 ℃ for different durations in a one-pass-processed sample.

3.2.4. Fractography

Fractographic examination of the fracture surfaces established a clear relationship between the interface microstructure and the dominant failure modes, as illustrated in Figures 10 and 11, and summarized in Table 2. In high passes, optimally annealed samples (4 passes at 400 °C for 1 h), failure proceeded cooperatively without macroscopic delamination. The Cu layer exhibited a dimpled rupture, which is a sign of microvoid coalescence and indicates a ductile fracture. In contrast, the Al layer presented a mixed-mode fracture, primarily characterized by cleavage-like facets mixed with dimples, suggesting a predominantly brittle behavior. The IMC layer, in turn, showed brittle intergranular fracture. Energy-dispersive spectroscopy (EDS) analysis further revealed that cracks predominantly initiated and propagated through the AlCu phase.

In contrast, low-pass, optimally annealed samples (1 pass at 400 °C for 1 h) failed primarily via interfacial delamination, with both Cu and Al layers displaying fully dimpled fracture surfaces that underscored their intrinsic ductility. The failure path followed the IMC layer, specifically through the AlCu phase. These observations highlight that a robust metallurgical bond suppresses macroscopic

 doi:10.20944/preprints202601.0095.v1

delamination, yet the fracture locus and overall plasticity remain governed by the intrinsic properties of the IMC layer. Notably, the AlCu phase serves as the preferred site for crack initiation, with wavy interfaces in low-pass materials exacerbating stress concentrations and thereby accelerating cracking within this brittle phase.

High-pass optimal annealing (4 passes, 400 °C/1 h) yields cooperative fracture delamination, with ductile Cu dimples (microvoid coalescence), mixed Al cleavage/dimples, and brittle IMC intergranular paths through AlCu. Whereas, low-pass (1 pass) promotes delamination along AlCu despite ductile layers, exacerbated by wavy stress risers. Robust bonding suppresses gross separation, but AlCu brittleness dictates locus, with geometry modulating propagation. These modes affirm interface-controlled failure, where topography governs initiation and IMC properties limit ductility. This is consistent with existing research on stress concentration in wavy clads that accelerates brittle phase cracking, suggesting that having a minimal sufficient IMCs can improve toughness [66].

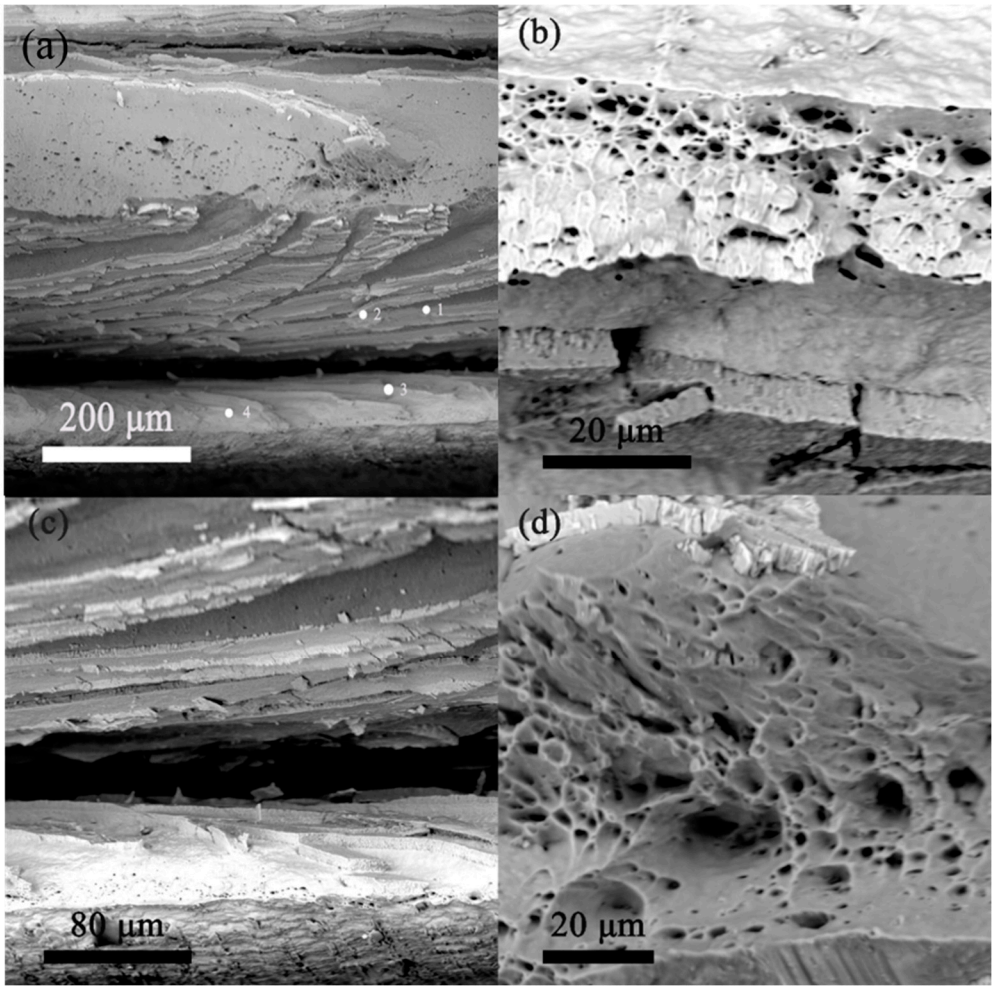

Figure 10. Fractography after annealing at 400 ℃ for 1 hour in 4-pass rolling: (a) fracture surface morphology of the material with EDS point numbers, (b) dimple in the copper layer, (c) fracture morphology of the interface layer, and (d) dimple in the aluminum layer.

 doi:10.20944/preprints202601.0095.v1

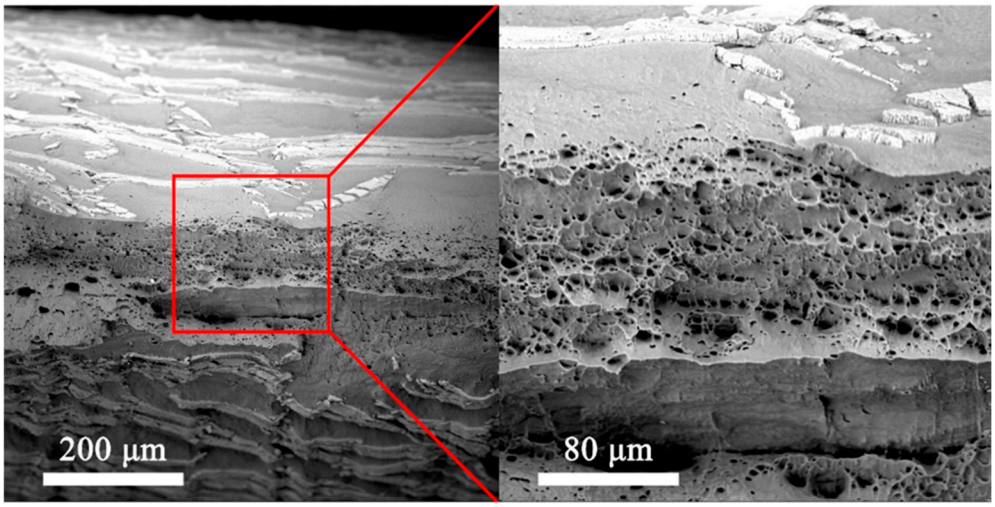

Figure 11. Fracture surface morphology and the magnified morphology of the aluminum layer dimples after annealing at 400 ℃ for 1 hour in 1-pass rolling.

Table 2. EDS point scanning composition analysis of the fracture surface of the material annealed at 400 ℃ for 1 hour in 1-pass rolling.

Spot	Element	Atomic Concentration	Components
1	Al	61.16	Al_2Cu
	Cu	38.84	
2	Al	51.19	AlCu
	Cu	48.81	
3	Al	51.59	AlCu
	Cu	48.41	
4	Al	39.16	Al_4Cu_9
	Cu	60.74	

4. Conclusions

This investigation systematically delineates the coupled thermomechanical pathways governing interfacial evolution and mechanical optimization in Cu18150/Al1060/Cu18150 trilayer composites fabricated via high-temperature oxygen-free rolling followed by tailored annealing. Rolling passes emerge as the primary architects of interfacial topography; low passes (1 pass sample) result in wavy, defect-rich interfaces that promote increased post-annealing diffusion because of the higher surface area. In contrast, high passes (4-pass sample) create flatter surfaces at the expense of IMC continuity but have little effect on the thickness of the as-rolled IMC (~2 μm). This highlights the significant role of deformation in shaping defect landscapes rather than influencing diffusion during transient rolling contacts.

Annealing plays a crucial role in transforming the bonding process from mechanical to metallurgical. The temperature range of 300-450 °C significantly influences the IMC growth, which can thicken exponentially from 2 to 18 μm, following parabolic kinetics with an activation energy of approximately 121-138 kJ/mol. This process illustrates a shift in mechanisms, starting with dislocation-pipe diffusion at shorter times and transitioning to lattice-controlled diffusion. Additionally, the time factor, particularly at 420 °C over 0.5 to 2 hours, leads to a non-linear densification pattern, where the thickness varies from 11.5 to 10.4 and then to 14.0 μm, primarily due to the annihilation of defects.

The mechanical performance highlights important microstructural factors: the as-rolled state enhances UTS from 250 to 344 MPa but significantly reduces ductility, dropping from 18.3% to 1.2%. In contrast, annealing improves elongation, achieving values greater than 20-28% through recovery

 doi:10.20944/preprints202601.0095.v1

and bonding processes. The optimal condition occurs at a single-pass treatment of 420 °C for 1 hour, resulting in a UTS of 258.9 MPa and an elongation of 28.2%. This condition leads to the fabrication of a uniform trilayer IMC of approximately 10.4 μm (Al_2Cu/AlCu/Al_4Cu_9), which effectively balances strength and ductility without leading to brittle overgrowth.

Fractographic revelations cement the AlCu phase as the Achilles' heel, dictating where cracks begin in ductile layers. The presence of low-pass waviness increases the likelihood of delamination due to stress concentrations, while high-pass flatness facilitates cooperative fracture. This affirms the role of interface-controlled failure, where topography modulates propagation and IMC brittleness sets limits of ductility. The findings establish a continuum that connects process, structure, and property, highlighting that the optimal conditions for exceeding benchmarks (≥220 MPa UTS and ≥20% EL) involve 1-pass HTOR followed by annealing at 420 °C for 1 hour. Additionally, they shed light on the specific characteristics of the alloy Cu18150, particularly the influence of Cr-Zr on diffusion stability.

Author Contributions: Conceptualization, Mahmoud Ebrahimi and Yuchao Zhao; Formal analysis, Yuchao Zhao and Linfeng Wu; Funding acquisition, Qudong Wang; Investigation, Mahmoud Ebrahimi and Shokouh Attarilar; Methodology, Shokouh Attarilar; Project administration, Qudong Wang; Resources, Qudong Wang; Supervision, Qudong Wang; Validation, Mahmoud Ebrahimi; Writing – original draft, Mahmoud Ebrahimi, Yuchao Zhao, Linfeng Wu, Shokouh Attarilar; Writing – review & editing, Mahmoud Ebrahimi, Yuchao Zhao, Shokouh Attarilar, and Qudong Wang. All authors have read and agreed to the published version of the manuscript.

Funding: This work was financially supported by the National Key Research and Development Program of China (Grant Nos. 2021YFB3701303 and 2024YFB3714303), the National Natural Science Foundation of China (No. U1902220), and the SJTU-Warwick Joint Seed Fund (Nos. SJTU2210 and SJTU2024).

Data Availability Statement: All data generated or analyzed during this study are included in this published article.

Conflicts of Interest: The authors declare no conflicts of interest.

References

1. Ebrahimi, M.; Luo, B.; Wang, Q.; Attarilar, S. High-Performance Nanoscale Metallic Multilayer Composites: Techniques, Mechanical Properties and Applications. *Materials (Basel).* **2024**, *17*, 2124, doi:10.3390/ma17092124.
2. Gao, H.; Li, J.; Lei, G.; Song, L.; Kong, C.; Yu, H. High Strength and Thermal Stability of Multilayered Cu/Al Composites Fabricated Through Accumulative Roll Bonding and Cryorolling. *Metall. Mater. Trans. A* **2022**, *53*, 1176–1187, doi:10.1007/s11661-022-06610-8.
3. Han, J.; Li, S.; Gao, X.; Huang, Z.; Wang, T.; Huang, Q. Effect of Annealing Process on Interface Microstructure and Mechanical Property of the Cu/Al Corrugated Clad Sheet. *J. Mater. Res. Technol.* **2023**, *23*, 284–299, doi:10.1016/j.jmrt.2022.12.188.
4. Ebrahimi, M.; Luo, B.; Wang, Q.; Attarilar, S. Enhanced Multifaceted Properties of Nanoscale Metallic Multilayer Composites. *Materials (Basel).* **2024**, *17*, 4004, doi:10.3390/ma17164004.
5. Zhang, W.; Huang, L.; Mi, X.; Xie, H.; Feng, X.; Ahn, J.H. Researches for Higher Electrical Conductivity Copper-based Materials. *cMat* **2024**, *1*, doi:10.1002/cmt2.13.
6. Watari, T.; Nansai, K.; Nakajima, K. Major Metals Demand, Supply, and Environmental Impacts to 2100: A Critical Review. *Resour. Conserv. Recycl.* **2021**, *164*, 105107, doi:10.1016/j.resconrec.2020.105107.
7. Valero, A.; Valero, A.; Calvo, G.; Ortego, A. Material Bottlenecks in the Future Development of Green Technologies. *Renew. Sustain. Energy Rev.* **2018**, *93*, 178–200, doi:10.1016/j.rser.2018.05.041.
8. Czerwinski, F. Aluminum Alloys for Electrical Engineering: A Review. *J. Mater. Sci.* **2024**, *59*, 14847–14892, doi:10.1007/s10853-024-09890-0.

 doi:10.20944/preprints202601.0095.v1

9. Chang, Q.; Gao, P.; Zhang, J.; Huo, Y.; Zhang, Z.; Xie, J. Numerical Simulation of Copper-Aluminum Composite Plate Casting and Rolling Process and Composite Mechanism. *Materials (Basel).* **2022**, *15*, 8139, doi:10.3390/ma15228139.
10. Ahmadzadeh Salout, S.; Mirbagheri, S.M.H. Microstructural and Mechanical Characterization of Al/Cu Interface in a Bimetallic Composite Produced by Compound Casting. *Sci. Rep.* **2024**, *14*, 7529, doi:10.1038/s41598-024-57849-7.
11. Saberi, Y.; Oveisi, H. Development of Novel Cellular Copper–Aluminum Composite Materials: The Advantage of Powder Metallurgy and Mechanical Milling Approach for Lighter Heat Exchanger. *Mater. Chem. Phys.* **2022**, *279*, 125742, doi:https://doi.org/10.1016/j.matchemphys.2022.125742.
12. Cai, H.; Wang, Q.; Zhang, N.; Ebrahimi, M.; Zhao, Y. Shear Behavior of Cu / Al / Cu Trilayered Composites Prepared by High-Temperature Oxygen-Free Rolling. *J. Alloys Compd.* **2024**, *1004*, 175857, doi:10.1016/j.jallcom.2024.175857.
13. Zhida, J.; Yangyang, X.U.; Jiaxin, Y.U.; Wencai, L.I.U.; Haowen, Z.H.U. Mechanical and Conductive Properties of Cu / 1060Al / Cu Three- Layer Composite Prepared by High-Temperature Oxygen-Free Rolling. *Acta Met. Sin* **2025**, *1*, doi:10.11900/0412.1961.2025.00057.
14. Jiang, Z.; Zhu, H.; Sun, J.; Huang, Y.; Wu, G.; Shang, Z.; Liu, W. Microstructure and Mechanical Properties of High-Temperature Free-Oxygen Rolled Cu/1060Al Bimetallic Composite Materials. *J. Mater. Res. Technol.* **2024**, *29*, 1262–1277, doi:10.1016/j.jmrt.2024.01.184.
15. Zhuo, X.; Shao, C.; Zhang, P.; Hu, Z.; Liu, H. Effect of Hot Rolling on the Microstructure and Mechanical Performance of a Mg-5Sn Alloy. *Materials (Basel).* **2022**, *15*, 5973, doi:10.3390/ma15175973.
16. Wilde, G.; Divinski, S. Grain Boundaries and Diffusion Phenomena in Severely Deformed Materials. *Mater. Trans.* **2019**, *60*, 1302–1315, doi:10.2320/matertrans.MF201934.
17. Beke, D.L.; Kaganovskii, Y.; Katona, G.L. Interdiffusion along Grain Boundaries – Diffusion Induced Grain Boundary Migration, Low Temperature Homogenization and Reactions in Nanostructured Thin Films. *Prog. Mater. Sci.* **2018**, *98*, 625–674, doi:10.1016/j.pmatsci.2018.07.001.
18. Kelly, M.B.; Niverty, S.; Chawla, N. Four Dimensional (4D) Microstructural Evolution of Cu6Sn5 Intermetallic and Voids under Electromigration in Bi-Crystal Pure Sn Solder Joints. *Acta Mater.* **2020**, *189*, 118–128, doi:10.1016/j.actamat.2020.02.052.
19. Zhao, Y.; Ebrahimi, M.; Attarilar, S.; Lu, Q.; Jiang, H.; Wang, Q. Layer Thickness Effects on Residual Stress , Microstructure , and Tensile Properties of Cu18150 / Al1060 / Cu18150 Multilayered Composites : An Integrated EBSD-KAM Approach. **2025**, 1–20.
20. Cai, H.; Yang, S.; Wang, Q.; Zhao, Y.; Jia, Q.; Ebrahimi, M.; Liu, L.; Guo, F.; Shang, Z. Interfacial Shear Fracture Behavior of C18150Cu/1060Al/C18150Cu Trilayered Composite at Different Temperatures. *Materials (Basel).* **2025**, *18*, doi:10.3390/ma18030559.
21. Xuan, Y.; Li, J.; Gao, H.; Yu, H. Tensile Properties of Cryorolled Cu/Al Clad Sheet with an SUS304 Interlayer after Annealing at Various Temperatures. *Materials (Basel).* **2024**, *17*, 4065, doi:10.3390/ma17164065.
22. Kim, D.; Kim, K.; Kwon, H. Interdiffusion and Intermetallic Compounds at Al/Cu Interfaces in Al-50vol.%Cu Composite Prepared by Solid-State Sintering. *Materials (Basel).* **2021**, *14*, 4307, doi:10.3390/ma14154307.
23. Zhao, D.; Guo, W.; Shang, Z.; Xu, C.; Gao, X.; Wang, X. The Growth Behavior and Kinetics of Intermetallic Compounds in Cu–Al Interface at 600°C–800 °C. *Intermetallics* **2024**, *168*, 108244, doi:10.1016/j.intermet.2024.108244.
24. Kim, D.-G.; Jung, S.-B. Interfacial Reactions and Growth Kinetics for Intermetallic Compound Layer between In–48Sn Solder and Bare Cu Substrate. *J. Alloys Compd.* **2005**, *386*, 151–156, doi:10.1016/j.jallcom.2004.05.055.
25. Zhao, N.; Zhong, Y.; Huang, M.L.; Ma, H.T.; Dong, W. Growth Kinetics of Cu6Sn5 Intermetallic Compound at Liquid-Solid Interfaces in Cu/Sn/Cu Interconnects under Temperature Gradient. *Sci. Rep.* **2015**, *5*, 13491, doi:10.1038/srep13491.
26. Yuan, Z.; Lu, Y.; Tu, Y.; Yuan, T.; Wang, X.; Ni, Z.; Wei, L.; Ali Raza, S.R. An Insight into the Interfacial Structure and Mechanical Properties of Al/Cu Laminated Sheets through Post-Treatment. *Vacuum* **2025**, *240*, 114542, doi:10.1016/j.vacuum.2025.114542.

 doi:10.20944/preprints202601.0095.v1

27. Fu, X.; Wang, R.; Zhu, Q.; Wang, P.; Zuo, Y. Effect of Annealing on the Interface and Mechanical Properties of Cu-Al-Cu Laminated Composite Prepared with Cold Rolling. *Materials (Basel).* **2020**, *13*, 369, doi:10.3390/ma13020369.
28. Mao, Z.; Xie, J.; Wang, A.; Wang, W.; Ma, D.; Liu, P. Effects of Annealing Temperature on the Interfacial Microstructure and Bonding Strength of Cu/Al Clad Sheets Produced by Twin-Roll Casting and Rolling. *J. Mater. Process. Technol.* **2020**, *285*, 116804, doi:10.1016/j.jmatprotec.2020.116804.
29. Gao, H.; Gu, H.; Wang, S.; Xuan, Y.; Yu, H. Effect of Annealing Temperature on the Interfacial Microstructure and Bonding Strength of Cu/Al Clad Sheets with a Stainless Steel Interlayer. *Materials (Basel).* **2022**, *15*, 2119, doi:10.3390/ma15062119.
30. Li, X.; Zhang, H.; Wang, J.; Yu, G.; Jiang, Z. Effect of Annealing Holding Time on Microstructure, Interface Diffusion Behavior, and Deformation Behavior of Cu/Al Composite Foil After Secondary Micro-Rolling. *Materials (Basel).* **2025**, *18*, 5418, doi:10.3390/ma18235418.
31. Sedighi, M.; Joudaki, J.; Kheder, H. Residual Stresses Due to Roll Bending of Bi-Layer Al-Cu Sheet: Experimental and Analytical Investigations. *J. Strain Anal. Eng. Des.* **2017**, *52*, 102–111, doi:10.1177/0309324716689442.
32. Wang, Z.; Bian, Y.; Yang, M.; Ma, R.; Fan, Y.; Du, A.; Zhao, X.; Cao, X. Investigation of Coordinated Behavior of Deformation at the Interface of Cu–Al Laminated Composite. *J. Mater. Res. Technol.* **2023**, *24*, 6545–6557, doi:10.1016/j.jmrt.2023.04.254.
33. LEE, S.; LEE, M.-G.; LEE, S.-P.; LEE, G.-A.; KIM, Y.-B.; LEE, J.-S.; BAE, D.-S. Effect of Bonding Interface on Delamination Behavior of Drawn Cu/Al Bar Clad Material. *Trans. Nonferrous Met. Soc. China* **2012**, *22*, s645–s649, doi:10.1016/S1003-6326(12)61779-8.
34. Sas-Boca, I.-M.; Iluțiu-Varvara, D.-A.; Tintelecan, M.; Aciu, C.; Frunză, D.I.; Popa, F. Studies on Hot-Rolling Bonding of the Al-Cu Bimetallic Composite. *Materials (Basel).* **2022**, *15*, 8807, doi:10.3390/ma15248807.
35. Ebrahimi, M.; Liu, G.; Li, C.; Wang, Q.; Jiang, H.; Ding, W.; Su, F.; Shang, Z. Characteristic Investigation of Trilayered Cu/Al8011/Al1060 Composite: Interface Morphology, Microstructure, and in-Situ Tensile Deformation. *Prog. Nat. Sci. Mater. Int.* **2021**, *31*, 679–687, doi:10.1016/j.pnsc.2021.08.005.
36. Ebrahimi, M.; Liu, G.; Li, C.; Wang, Q.; Jiang, H.; Ding, W.; Su, F. Experimental and Numerical Analysis of Cu/Al8011/Al1060 Trilayered Composite: A Comprehensive Study. *J. Mater. Res. Technol.* **2020**, *9*, 14695–14707, doi:10.1016/j.jmrt.2020.10.031.
37. Ebrahimi, M.; Liu, G.; Wang, Q.; Jiang, H.; Ding, W.; Shang, Z.; Luo, L. Evaluation of Interface Structure and High-Temperature Tensile Behavior in Cu/Al8011/Al5052 Trilayered Composite. *Mater. Sci. Eng. A* **2020**, *798*, 140129, doi:10.1016/j.msea.2020.140129.
38. Zheng, H.; Zhang, R.; Xu, Q.; Kong, X.; Sun, W.; Fu, Y.; Wu, M.; Liu, K. Fabrication of Cu/Al/Cu Laminated Composites Reinforced with Graphene by Hot Pressing and Evaluation of Their Electrical Conductivity. *Materials (Basel).* **2023**, *16*, 622, doi:10.3390/ma16020622.
39. Han, M.; Li, Z.; Huang, Z.; Wang, X.; Gao, W. Thermal Mechanical Bending Response of Symmetrical Functionally Graded Material Plates. *Materials (Basel).* **2023**, *16*, 4683, doi:10.3390/ma16134683.
40. Cai, H.; Wang, Q.; Zhang, N.; Ebrahimi, M.; Zhao, Y.; Liu, L.; Guo, F. Shear Behavior of Cu/Al/Cu Trilayered Composites Prepared by High-Temperature Oxygen-Free Rolling. *J. Alloys Compd.* **2024**, *1004*, 175857, doi:10.1016/j.jallcom.2024.175857.
41. de Leon, M.; Shin, H.-S. Review of the Advancements in Aluminum and Copper Ultrasonic Welding in Electric Vehicles and Superconductor Applications. *J. Mater. Process. Technol.* **2022**, *307*, 117691, doi:10.1016/j.jmatprotec.2022.117691.
42. Liang, X.L.; Liu, D.Y.; Shen, Z.L.; Tao, N.R. Enhanced Precipitation Hardening in Nanograined CuCrZr Alloy. *Scr. Mater.* **2024**, *247*, 116118, doi:10.1016/j.scriptamat.2024.116118.
43. Zeng, C.; Wen, H.; Bernard, B.C.; Raush, J.R.; Gradl, P.R.; Khonsari, M.; Guo, S.M. Effect of Temperature History on Thermal Properties of Additively Manufactured C-18150 Alloy Samples. *Manuf. Lett.* **2021**, *28*, 25–29, doi:10.1016/j.mfglet.2021.02.002.
44. Li, S.; Wang, W.; Cui, Y.; Xie, J.; Wang, A.; Mao, Z.; Zhang, F. Trace Zr Addition Enhances Strength and Plasticity in Cu-Zr/Al2Cu/Al Alloys via Local FCC-to-BCC Transition: Molecular Dynamics Insights on

 doi:10.20944/preprints202601.0095.v1

Interface-Specific Deformation and Strain Rate Effects. *Materials (Basel).* **2025**, *18*, 1480, doi:10.3390/ma18071480.

45. Chen, D.; Kang, L.; Wang, X.; Zhou, H.; Liu, Z.; Xu, Y.; Liu, D.; Yao, P. The Diffusion Behavior and Mechanical Properties of CuCrZr/AlMgSi Interaction Layer in Ultra-High Speed Sliding Electrical Contact. *J. Alloys Compd.* **2025**, *1029*, 180628, doi:10.1016/j.jallcom.2025.180628.
46. Wang, D.; Lv, J.; Liu, Z.; Liu, L.; Wei, Y.; Chang, C.; Zhou, W.; Zhang, Y.; Han, C. Interface Optimization, Microstructural Characterization, and Mechanical Performance of CuCrZr/GH4169 Multi-Material Structures Manufactured via LPBF-LDED Integrated Additive Manufacturing. *Materials (Basel).* **2025**, *18*, 2206, doi:10.3390/ma18102206.
47. Wang, J.; Zhao, F.; Xie, G.; Hou, Y.; Wang, R.; Liu, X. Rolling Deformation Behaviour and Interface Evaluation of Cu-Al Bimetallic Composite Plates Fabricated by Horizontal Continuous Composite Casting. *J. Mater. Process. Technol.* **2021**, *298*, 117296, doi:10.1016/j.jmatprotec.2021.117296.
48. Lee, J.; Jeong, H. Intermetallic Formation at Interface of Al/Cu Clad Fabricated by Hydrostatic Extrusion and Its Properties. *J. Nanosci. Nanotechnol.* **2015**, *15*, 8589–8592, doi:10.1166/jnn.2015.11494.
49. Yang, D.; Huang, Y. Interfacial Intermetallic Compound Modification to Extend the Electromigration Lifetime of Copper Pillar Joints. *Front. Mater.* **2023**, *9*, doi:10.3389/fmats.2022.1080848.
50. Chang, Q.; Zhang, J.; Gao, P.; Zhang, Z.; Huo, Y.; Xie, J. Study on the Phase Structure of the Interface Zone of Cu–Al Composite Plate in Cast-Rolling State and Different Heat Treatment Temperatures Based on EBSD. *J. Mater. Res. Technol.* **2023**, *24*, 1056–1069, doi:10.1016/j.jmrt.2023.03.063.
51. Hang, C.J.; Wang, C.Q.; Mayer, M.; Tian, Y.H.; Zhou, Y.; Wang, H.H. Growth Behavior of Cu/Al Intermetallic Compounds and Cracks in Copper Ball Bonds during Isothermal Aging. *Microelectron. Reliab.* **2008**, *48*, 416–424, doi:10.1016/j.microrel.2007.06.008.
52. Zechner, J.; Kolednik, O. Fracture Resistance of Aluminum Multilayer Composites. *Eng. Fract. Mech.* **2013**, *110*, 489–500, doi:10.1016/j.engfracmech.2012.11.007.
53. Yousefi Mehr, V.; Toroghinejad, M.R. Mode Ⅰ Fracture Analysis of Aluminum-Copper Bimetal Composite Using Finite Element Method. *Heliyon* **2024**, *10*, e26329, doi:10.1016/j.heliyon.2024.e26329.
54. Cai, H.; Yang, S.; Wang, Q.; Zhao, Y.; Jia, Q.; Ebrahimi, M.; Liu, L.; Guo, F.; Shang, Z. Interfacial Shear Fracture Behavior of C18150Cu/1060Al/C18150Cu Trilayered Composite at Different Temperatures. *Materials (Basel).* **2025**, *18*, 559, doi:10.3390/ma18030559.
55. Gao, H.; Li, J.; Song, L.; Peng, X.; Kong, C.; Yu, H. Effect of Intermetallic Compounds on the Mechanical Properties of Cu/Al Clad Sheets with an SS304 Interlayer. *Mater. Sci. Eng. A* **2024**, *915*, 147286, doi:10.1016/j.msea.2024.147286.
56. Mypati, O.; Pal, S.K.; Srirangam, P. Tensile and Fatigue Properties of Aluminum and Copper Micro Joints for Li-Ion Battery Pack Applications. *Forces Mech.* **2022**, *7*, 100101, doi:10.1016/j.finmec.2022.100101.
57. Hatano, R.; Ogura, T.; Matsuda, T.; Sano, T.; Hirose, A. Relationship between Intermetallic Compound Layer Thickness with Deviation and Interfacial Strength for Dissimilar Joints of Aluminum Alloy and Stainless Steel. *Mater. Sci. Eng. A* **2018**, *735*, 361–366, doi:10.1016/j.msea.2018.08.065.
58. Wang, Z.; Zhu, X.; Wang, C.; Xiao, X.; Zhang, K.; Jiang, C.; Liu, J. Microstructure and Mechanical Properties of Al/Cu-SS Hybrid Composite via Ball Milling and Friction Stir Processing. *iScience* **2025**, *28*, 114008, doi:10.1016/j.isci.2025.114008.
59. Yu, Q.; Wang, J.; Zheng, Z.; Mai, Y. Study on Mechanical and Electrical Properties of Layered CuCrZr/Cu-Al2O3 Composite. *Mater. Today Commun.* **2025**, *43*, 111826, doi:10.1016/j.mtcomm.2025.111826.
60. Ma, Y.; Chen, H.; Li, H.; Dang, S. Influence Mechanism of Ageing Parameters of Cu-Cr-Zr Alloy on Its Structure and Properties. *Materials (Basel).* **2022**, *15*, 7605, doi:10.3390/ma15217605.
61. Chen, J.; Zhou, D.; Zhou, X.; Liang, H.; Feng, P.; Yu, Y.; Kang, X. Investigation of Interface Characteristics and Mechanical Performances of Cu/Al Plate Fabricated by Underwater Explosive Welding Method. *PLoS One* **2025**, *20*, e0320970, doi:10.1371/journal.pone.0320970.
62. Song, G.; Li, T.; Yu, J.; Liu, L. A Review of Bonding Immiscible Mg/Steel Dissimilar Metals. *Materials (Basel).* **2018**, *11*, 2515, doi:10.3390/ma11122515.

 doi:10.20944/preprints202601.0095.v1

63. Ebrahimi, M.; Zhao, Y.; Cai, H.; Attarilar, S.; Shang, Z.; Wang, Q. Interface Characterization of Cu18150/Al1060/Cu18150 Laminated Composite Produced by Combined Cast-Roll and Hot-Roll Technique. *J. Mater. Res. Technol.* **2025**, *36*, 7111–7124, doi:10.1016/j.jmrt.2025.05.005.
64. Wang, W.; Wang, H.; Liu, X.; Liu, Z. Interface Evolution and Strengthening of Two-Step Roll Bonded Copper/Aluminum Clad Composites. *Mater. Charact.* **2023**, *199*, 112778, doi:10.1016/j.matchar.2023.112778.
65. Chen, C.-Y.; Hwang, W.-S. Effect of Annealing on the Interfacial Structure of Aluminum-Copper Joints. *Mater. Trans.* **2007**, *48*, 1938–1947, doi:10.2320/matertrans.MER2006371.
66. Yang, D.; Wang, A.; Ma, D.; Mao, Z.; Wang, J.; Liang, T.; Xie, J. Interface Evolution and Properties of C18150 Cu/1060 Al Composites in the Process of Annealing. *J. Alloys Compd.* **2025**, *1010*, 178171, doi:10.1016/j.jallcom.2024.178171.